Eur. Phys. J. D **13**, 213–220 (2001)

THE EUROPEAN PHYSICAL JOURNAL D

EDP Sciences

Photoionization of atoms in parallel electric and magnetic fields: Cross-section calculations using the Lanczos algorithm and the complex coordinate method in a discrete variable representation

H. Suno[1,a], L. Andric[1], T.P. Grozdanov[1,2], and R. McCarroll[1]

[1] Laboratoire de Dynamique des Ions, Atomes et Molécules[b], Université Pierre et Marie Curie, 4 place Jussieu T12-B75, 75252 Paris Cedex 05, France
[2] Institute of Physics, P.O. Box 57, 11001 Belgrade, Yugoslavia

Received 15 May 2000 and Received in final form 4 October 2000

Abstract. A combination of the complex-coordinate method and the Lanczos recursion scheme is implemented in the discrete variable representation (DVR) to obtain total photoionization cross-sections using an iterative procedure. Applications to photoionization of hydrogen atoms in electric fields and sodium atoms in electric and parallel electric and magnetic fields are presented and discussed.

PACS. 32.60.+i Zeeman and Stark effects – 32.80.Fb Photoionization of atoms and ions

1 Introduction

The photoionization of simple atomic systems in external fields is most successfully treated using methods based on the complex coordinate (scaling, dilatation, or rotation) method (for a review see, for example [1]). In this approach, the total photoionization cross-section can be expressed in terms of complex eigenvalues of the complex scaled Hamiltonian and complex dipole matrix elements (*i.e.* poles and residues of the complex scaled Green function) [2]. The first applications treated hydrogen atoms in external fields [3–5]. Further extensions for the treatment of non hydrogenic systems, such as alkali-metal atoms, have been developed by combining the complex coordinate method with R-matrix theory [6,7].

In the present work, we apply a combination of the complex coordinate method and the complex version [8] of the Lanczos algorithm [9] in iterative calculations of total photoionization cross-sections. In this approach, the cross-section is expressed as a continued fraction whose coefficients are directly obtained from Lanczos iterations [8,10,11], thus avoiding explicit calculations of individual poles and residues of the complex scaled Green function. Similar ideas have been developed previously in calculations of the photoionization cross-sections of a hydrogen atom in an external electric [11] and crossed electric and magnetic fields [12].

The novelty in the present work is the use of a discrete variable representation (DVR) [13] of the complex scaled Hamiltonian. Loosely speaking, a DVR is an approximate, discretized coordinate representation in which the potential-energy matrix is diagonal. Thus the extension to alkali-metal atoms is trivial when using DVR and model core-potentials. For many one-dimensional DVR's, differential operators (kinetic energy) matrix elements are analytically known (see [14] where the term "Lagrange mesh" is used to describe a DVR). For simple, effectively one-dimensional, problems of photoionization of hydrogen and alkali-metal atoms in the absence of external fields our method has recently been successfully tested [15]. In multidimensional problems like those treated in the present work, direct-products of one-dimensional DVR's lead to sparse kinetic energy matrices, which is very desirable when using iterative methods. Previously, we have used appropriate DVR for studying the properties of bound and quasi-bound atomic Rydberg states in external fields [16,17].

The plan of the paper is as follows. In Section 2, we explain our method and give all necessary formulae for calculating the total photoionization cross-sections. All applications are described in Section 3. First, we calculate the photoionization cross-section of a hydrogen atom in an electric field for π polarization. Next, we apply our method to photoionization of sodium atoms in an electric field induced by a stepwise transition by two laser pulses for various combinations of photon polarizations. We also study the evolution of sodium-atom spectra in parallel electric and magnetic fields as a function of increasing magnetic field strength. Concluding remarks are given in Section 4. We use atomic units throughout the work except where explicitly stated otherwise.

[a] e-mail: suno@diam.jussieu.fr
[b] ESA 7066 du CNRS

2 Method

2.1 Lanczos algorithm and complex coordinate method

Designating $\boldsymbol{\mu}$ as the dipole operator, $\hat{\boldsymbol{\epsilon}}$ as the polarization vector of the radiation and $|\Psi_i\rangle$ as the initial bound-state vector with energy E_i, the total cross-section for atomic photoionization can be represented in the following form (see, for example, [2]):

$$\sigma(E) = -\frac{4\pi\omega}{c}\mathrm{Im}\langle\Phi_i|\hat{G}(E^+)|\Phi_i\rangle, \tag{2.1}$$

where $|\Phi_i\rangle = \boldsymbol{\mu}\cdot\hat{\boldsymbol{\epsilon}}|\Psi_i\rangle$, $\omega = E - E_i$ and the Green operator is defined as

$$\hat{G}(E^+) = \lim_{\varepsilon\to 0+}(E + \mathrm{i}\varepsilon - \hat{H})^{-1}. \tag{2.2}$$

The Hamiltonian of the system, representing a hydrogen or (in one-electron approximation) an alkali-metal atom in parallel electric and magnetic fields is given by:

$$\hat{H} = -\frac{1}{2}\Delta - \frac{1}{r} + V_{\mathrm{core}}(r) + zF + \frac{1}{2}(l_z + 2s_z)B + \frac{1}{8}(x^2 + y^2)B^2, \tag{2.3}$$

where F and B are the electric and magnetic field strengths expressed in atomic units of $F_0 \approx 5.14 \times 10^6$ kV/cm and $B_0 \approx 2.35 \times 10^5$ T. $V_{\mathrm{core}}(r)$ is a model potential of the valence electron, added in the case of an alkali-metal atom. In the linear Zeeman term $l_z = m$ and $s_z = m_{\mathrm{s}}$ are conserved projections of the electronic orbital angular momentum and spin. In writing Hamiltonian (2.3) the relativistic effects (such as spin-orbit interaction) have been neglected, although, as will be discussed later in Section 3, when necessary they can be accounted for by means of the perturbation theory. Therefore, in this section we ignore spin variables and consider only the coordinate dependence of wavefunctions.

The next step is to reexpress equation (2.1) using the complex coordinate transformation [1]. It consists in replacing the electron position and momentum operators by complex quantities:

$$\mathbf{r} \to \mathbf{r}\mathrm{e}^{\mathrm{i}\theta}, \qquad \mathbf{p} \to \mathbf{p}\mathrm{e}^{-\mathrm{i}\theta}, \tag{2.4}$$

where θ is a real "rotation angle". The transformed Hamiltonian $\hat{H}(\theta)$ is a non-Hermitian operator and has a complex spectrum which can be related to the original Hamiltonian $\hat{H} = \hat{H}(\theta = 0)$. In general, the bound (real discrete) spectrum is common to both $\hat{H}$ and $\hat{H}(\theta)$ whereas the continua are rotated by the angle -2θ around their thresholds into the lower half of the complex energy plane. The resonances of $\hat{H}$ are the discrete complex eigenvalues of $\hat{H}(\theta)$ and are independent of θ provided they are uncovered by the rotation.

When using the complex coordinate method and the Lanczos algorithm, the usual scalar product is replaced by the pseudo-scalar product

$$(f(x)|g(x)) = \int f(x)g(x)\mathrm{d}x. \tag{2.5}$$

By transforming to complex coordinates and assuming that the initial state wavefunction is real, equation (2.1) can be rewritten as [2]:

$$\sigma(E) = -\frac{4\pi\omega}{c}\mathrm{Im}(\Phi_i^\theta|\hat{G}_\theta(E)|\Phi_i^\theta), \tag{2.6}$$

where $|\Phi_i^\theta)$ is the complex coordinate transform of $|\Phi_i)$, defined in the coordinate representation as

$$\Phi_i^\theta(\mathbf{r}) = \mathrm{e}^{\frac{3}{2}\mathrm{i}\theta}\Phi_i(\mathbf{r}\mathrm{e}^{\mathrm{i}\theta}) \tag{2.7}$$

and the transformed Green operator is given by:

$$\hat{G}_\theta(E) = [E - \hat{H}(\theta)]^{-1}. \tag{2.8}$$

In order to calculate the matrix element in equation (2.6) (the Green function) $G_{ii}(E) = (\Phi_i^\theta|\hat{G}_\theta(E)|\Phi_i^\theta)$, we adopt the Lanczos iteration scheme. This is defined by the recursive relation:

$$b_n|\phi_{n+1}) = \hat{H}(\theta)|\phi_n) - a_n|\phi_n) - b_{n-1}|\phi_{n-1}), \tag{2.9}$$

where $a_n = (\phi_n|\hat{H}(\theta)|\phi_n)$, $(\phi_n|\phi_{n'}) = \delta_{nn'}$ and b_n is chosen to normalize $|\phi_{n+1})$. In the "Lanczos basis": $\{|\phi_1), |\phi_2), ...\}$ the Hamiltonian $\hat{H}(\theta)$ is represented as a complex symmetric tridiagonal matrix with diagonal elements: $a_1, a_2, ...$ and off-diagonal elements: $b_1, b_2, ...$ Using then

$$|\phi_1) = (\Phi_i^\theta|\Phi_i^\theta)^{-1/2}|\Phi_i^\theta) \tag{2.10}$$

as a starting vector, the Green function can be written as [8,10,11]:

$$G_{ii}(E) \approx G_{ii}^N(E) = (\Phi_i^\theta|\Phi_i^\theta) \times [E - a_1 - b_1^2/(E - a_2 - b_2^2/(\cdots - b_{N-1}^2/(E - a_N)))]^{-1}, \tag{2.11}$$

where N is a sufficiently large number related to the desired degree of the convergence. In practice, the continued fraction in equation (2.11) is calculated as a ratio:

$$G_{ii}^N(E) = (\Phi_i^\theta|\Phi_i^\theta)\frac{A_N}{B_N}, \tag{2.12}$$

where A_N and B_N are defined recursively as [18]:

$$A_n = (E - a_n)A_{n-1} - b_{n-1}^2 A_{n-2}, \tag{2.13}$$

$$B_n = (E - a_n)B_{n-1} - b_{n-1}^2 B_{n-2}, \tag{2.14}$$

with the initial conditions:

$$A_1 = 1, \quad B_1 = E - a_1, \quad A_0 = 0, \quad B_0 = 1. \tag{2.15}$$

Finally, we find,

$$\sigma(E) \approx \sigma_N(E) = -\frac{4\pi\omega}{c}\mathrm{Im}\left[(\Phi_i^\theta|\Phi_i^\theta)\frac{A_N}{B_N}\right], \tag{2.16}$$

where A_N and B_N are calculated by using relations (2.9, 2.13, 2.14).

We note that due to the energy-independence of the Lanczos coefficients a_n and b_n, a single iteration procedure provides cross-sections at all energies. This is different from the traditional methods which require numerical calculation of the continuum wavefunction at each energy separately.

2.2 DVR basis functions and Hamiltonian matrix

The implementation of the method requires the choice of a finite basis to represent the (complex scaled) Hamiltonian and the state vectors of the system. Our choice is a DVR [13,14]. When using a DVR, numerical calculation of the matrix elements is avoided whatever the form of the interaction potential. The potential energy matrix is diagonal and trivial to calculate, while in multidimensional problems the kinetic energy matrix is sparse and matrix elements are analytically known. This is a desirable feature, because the most CPU-time consuming operation in the method is the matrix-vector multiplication in Lanczos recursion (2.9).

Due to the cylindrical symmetry of the Hamiltonian (2.3), in each particular case the integration over azimuthal angle can trivially be performed in expression (2.1), thus rendering the problem effectively two-dimensional. In order to describe the dynamics in the remaining two degrees of freedom, we shall use the scaled parabolic coordinates

$$\frac{u}{\lambda} = (\rho^2 + z^2)^{1/2} + z, \tag{2.17}$$

$$\frac{v}{\lambda} = (\rho^2 + z^2)^{1/2} - z, \tag{2.18}$$

$$\rho \mathrm{d}\rho \mathrm{d}z = \frac{1}{4\lambda^3}(u+v)\mathrm{d}u\mathrm{d}v, \tag{2.19}$$

where λ is an arbitrary scaling parameter.

After performing the transformation (2.4) the complex-rotated Hamiltonian, restricted to a subspace with fixed magnetic quantum number m and spin projection m_s, takes the form

$$\hat{H}(\theta) = \mathrm{e}^{-2\mathrm{i}\theta} T + V(u\mathrm{e}^{\mathrm{i}\theta}, v\mathrm{e}^{\mathrm{i}\theta}) \tag{2.20}$$

with

$$T = \frac{2\lambda^2}{u+v}\left[-\frac{\partial}{\partial u}u\frac{\partial}{\partial u} - \frac{\partial}{\partial v}v\frac{\partial}{\partial v} + \frac{m^2}{4}\left(\frac{1}{u}+\frac{1}{v}\right)\right], \tag{2.21}$$

$$V(u\mathrm{e}^{\mathrm{i}\theta}, v\mathrm{e}^{\mathrm{i}\theta}) = -\mathrm{e}^{-\mathrm{i}\theta}\frac{2\lambda}{u+v} + V_\mathrm{core}\left(\frac{u+v}{2\lambda}\mathrm{e}^{\mathrm{i}\theta}\right) + \mathrm{e}^{\mathrm{i}\theta}\frac{u-v}{2\lambda}F + \frac{B}{2}(m+2m_\mathrm{s}) + \mathrm{e}^{\mathrm{i}2\theta}\frac{B^2}{8\lambda^2}uv. \tag{2.22}$$

To represent the system Hamiltonian and state vectors, we adopt the two dimensional DVR basis, formed by the direct product of one-dimensional DVR basis functions [16]:

$$Y^{|m|}_{\alpha\beta}(u,v) = \frac{2\lambda^{3/2}}{(u_\alpha+v_\beta)^{1/2}} y^{|m|}_\alpha(u) y^{|m|}_\beta(v), \tag{2.23}$$

where

$$y^{|m|}_\alpha(u) = w_\alpha^{\frac{1}{2}} \sum_{k=o}^{n-1} \Phi^{|m|}_k(u_\alpha)\Phi^{|m|}_k(u) = w_\alpha^{-\frac{1}{2}} \left(\frac{\mathrm{d}\Phi^{|m|}_n(u_\alpha)}{\mathrm{d}u}\right)^{-1} \frac{\Phi^{|m|}_n(u)}{u-u_\alpha}, \quad \alpha = 1,2,...n, \tag{2.24}$$

and

$$\Phi^{|m|}_k(u) = \left[\frac{k!}{(k+|m|)!}\right]^{\frac{1}{2}} L^{|m|}_k(u) u^{\frac{|m|}{2}} \mathrm{e}^{-\frac{u}{2}}, \tag{2.25}$$

with (u_α, w_α), denoting generalized Gauss-Laguerre quadrature points and weights related to generalized Laguerre polynomials $L^{|m|}_k(u)$.

The DVR of the Hamiltonian is then given by

$$H(\theta)_{\alpha\beta,\alpha'\beta'} = \mathrm{e}^{-2\mathrm{i}\theta} T_{\alpha\beta,\alpha'\beta'} + V(u_\alpha \mathrm{e}^{\mathrm{i}\theta}, v_\beta \mathrm{e}^{\mathrm{i}\theta})\delta_{\alpha\alpha'}\delta_{\beta\beta'} \tag{2.26}$$

where

$$T_{\alpha\beta,\alpha'\beta'} = \frac{2\lambda^2(t^u_{\alpha\alpha'}\delta_{\beta\beta'} + \delta_{\alpha\alpha'}t^v_{\beta\beta'})}{(u_\alpha+v_\beta)^{1/2}(u_{\alpha'}+v_{\beta'})^{1/2}} \tag{2.27}$$

with [14]

$$t^u_{\alpha\alpha'} = \begin{cases} \frac{1}{3}\left(n + \frac{|m|+1}{2} - \frac{u_\alpha}{4} + \frac{m^2-1}{2u_\alpha}\right) & \alpha = \alpha' \\ \frac{2(-1)^{\alpha-\alpha'}(u_\alpha u_{\alpha'})^{\frac{1}{2}}}{(u_\alpha - u_{\alpha'})^2} & \alpha \neq \alpha'. \end{cases} \tag{2.28}$$

Matrix (2.26) has an explicitly sparse structure which can be exploited in order to develop an efficient matrix-vector multiplication code.

In the DVR defined above, any wavefunction $\chi(u,v)$ is represented by a vector whose components are given by

$$\chi_{\alpha\beta} = \left[\frac{(u_\alpha+v_\beta)w_\alpha w_\beta}{4\lambda^3}\right]^{1/2} \chi(u_\alpha, v_\beta). \tag{2.29}$$

3 Applications

The method described in the previous section is applied here to calculate total photoionization cross-sections of atoms in external fields. We begin with the photoionization of a hydrogen atom in an electric field. Secondly, we deal with sodium atoms in electric fields. Finally, we treat sodium atoms in parallel electric and magnetic fields.

3.1 Hydrogen atom in an electric field

We shall consider the photoionization from the parabolic state $(n_1 = 1, n_2 = 0, m = 0)$ of a hydrogen atom in an electric field of $F = 5.714$ kV/cm. The classical ionization threshold is located at $E = -2\sqrt{F}$ in a.u., that is $E \approx -462$ cm^{-1}. We treat the case of linear polarization parallel to the field direction (π – polarized photons). The dynamics in the $m = 0$ subspace is relevant and the initial wavefunction is given by

$$\Phi^\theta_i(u,v) = \mathrm{e}^{\mathrm{i}\theta}\frac{u-v}{2\lambda}\Psi^\theta_i(u,v), \tag{3.1}$$

where

$$\Psi_i^{\theta}(u,v) = \mathrm{e}^{\mathrm{i}3\theta/2}\Psi_{100}(u\mathrm{e}^{\mathrm{i}\theta}, v\mathrm{e}^{\mathrm{i}\theta}) = \mathrm{e}^{\mathrm{i}3\theta/2}\frac{1}{2^{3/2}}\left(1-\frac{u}{2\lambda}\mathrm{e}^{\mathrm{i}\theta}\right)\exp\left(-\frac{u+v}{4\lambda}\mathrm{e}^{\mathrm{i}\theta}\right) \quad (3.2)$$

is the complex-rotated hydrogenic parabolic ($n_1 = 1, n_2 = 0, m = 0$) state wavefunction. Here, we assume that the initial state is unperturbed by external fields.

At the bottom of Figure 1, we show the results of our calculations for the spectra above the classical ionization threshold in the region below and above the zero-field ionization threshold. These results are obtained by using the value of the rotation angle $\theta = 0.05$, the scaling parameter $\lambda = 0.03$, the number of DVR basis functions $N_{\mathrm{DVR}} = 70 \times 70 = 4\,900$ and the number of terms in the Lanczos recursion $N = 20\,000$. Here, and in all other cases we have checked that the results are stable with respect to variations of these parameters. Following Karlsson and Goscinski [11], when using equation (2.6) we have added a small imaginary part to the energy, that is, we have substituted $E \to E + \mathrm{i}\varepsilon$ with $\varepsilon = 0.01\,\mathrm{cm}^{-1}$. In this way all resonances get an additional width of 2ε, so that some very sharp resonances which would otherwise be very difficult to resolve, show up. Our results are in agreement with calculations of Karlsson and Goscinski [11] shown in the middle of Figure 1. Both results compare well with the experimental results of Rottke and Welge [20] shown at the top of Figure 1. In this comparison one should take into account that some very sharp lines are missing in the experimental results due to the difficulties of detecting very long lived states. The theoretical approach of Alvarez *et al.* [3] is based on summation of the contributions of individual resonances to the cross-section, so that the experimental situation can be simulated by eliminating contributions of the sharpest resonances. In addition, in our calculations we have neglected small admixture of parabolic ($n_1 = 0, n_2 = 1, m = 0$) state (1%) and ($n_1 = 0, n_2 = 0, m = 1$) state (3%) present in the realistic initial state [3].

Finally, we note that the number of DVR grid points (basis size) used in our calculations 4 900 is much smaller than the spherical basis size 22 500 of Karlsson and Goscinski [11]. This indicates that the use of the direct product of two DVRs related to parabolic coordinates provides an efficient and economical way to calculate the Stark spectra of atoms.

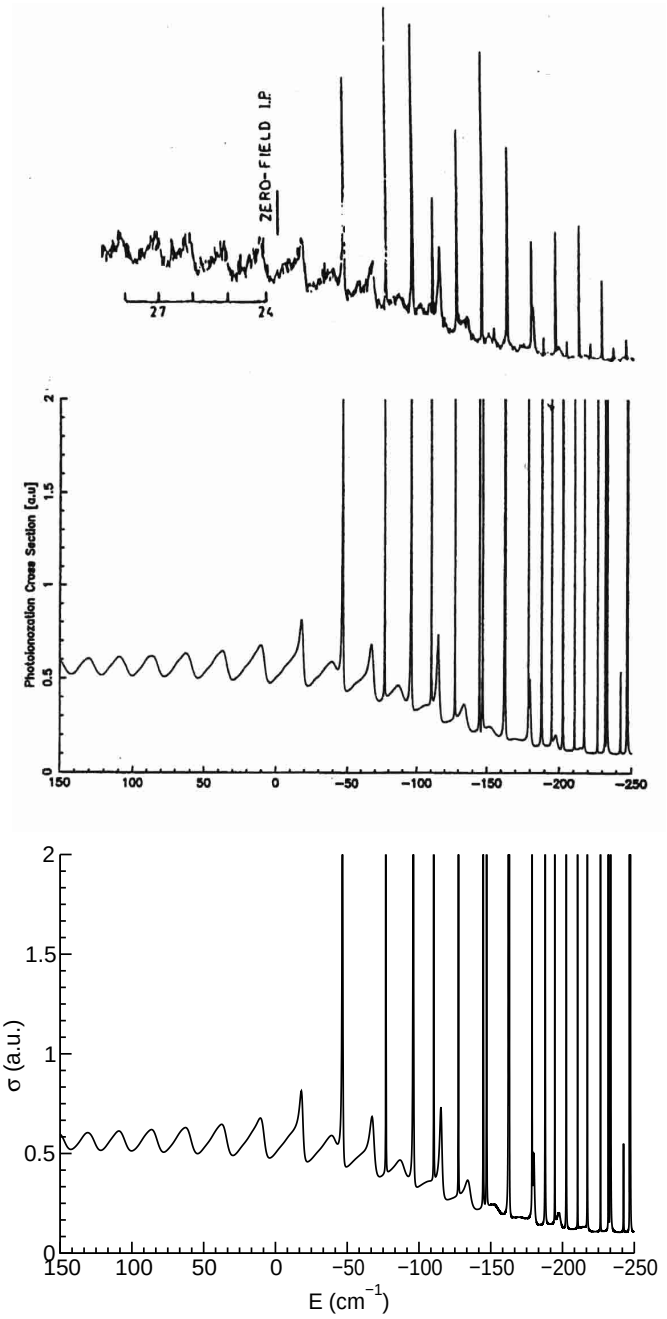

Fig. 1. Cross-sections for photoionization from the parabolic $(n_1, n_2, m) = (1, 0, 0)$ state of a hydrogen atom in an electric field of $F = 5.714$ kV/cm by linearly (π) polarized photons. From the bottom to the top: present results, calculation of Karlsson and Goscinski [11] and experiment [20].

3.2 Sodium atom in an electric field

To treat the case of a sodium atom, we introduce a model potential of the valence electron obtained by fitting the unperturbed spectra of the atom in the one-electron approximation [19]:

$$V_{\mathrm{core}}^{\mathrm{Na}}(r) = -\frac{10}{r}(\mathrm{e}^{-7.902r} + 2.351r\mathrm{e}^{-2.688r}). \quad (3.3)$$

We need to calculate the complex-rotated radial wavefunction of an initial unperturbed state of a sodium atom. To this end, we construct the matrix representing the complex-rotated radial Hamiltonian (see also Ref. [15]):

$$\hat{H}_0(\theta) = -\frac{\mathrm{e}^{-2\mathrm{i}\theta}}{2}\frac{\mathrm{d}^2}{\mathrm{d}r^2} + \mathrm{e}^{-2\mathrm{i}\theta}\frac{l(l+1)}{2r^2} - \frac{\mathrm{e}^{-\mathrm{i}\theta}}{r} + V_{\mathrm{core}}^{\mathrm{Na}}(r\mathrm{e}^{\mathrm{i}\theta}) \quad (3.4)$$

by using a one-dimensional DVR based on generalized Gauss-Laguerre quadrature [14]. The complex-rotated

wavefunction is obtained by diagonalizing this matrix. Subsequently, we use a linear interpolation to express it in the two-dimensional DVR introduced in the previous section.

We first consider a stepwise ionization by two laser pulses, which has been studied previously both, experimentally [21] and theoretically [7,22]. Both photons are linearly π-polarized and are absorbed by a sodium atom in an electric field of $F = 3.59$ kV/cm. The first photon excites the valence electron from the ground state to the $3p^2\mathrm{P}_{3/2}$ level, while the second ionizes the atom above the (classical) ionization threshold located at $E \approx -367\,\mathrm{cm}^{-1}$. The intermediate state, when represented in ls coupling, contains both $m = 0$ and $m = 1$ components in a fixed proportion. Here, and in all other cases considered below, the small (quadratic) Stark effect of the intermediate state is neglected. Thus, the cross-section for absorption of the second (ionizing) photon is a linear combination of the cross-sections for $m = 0 \to 0$ and $m = 1 \to 1$ transitions [22]:

$$\sigma_{3/2} = \frac{2}{3}\sigma(m = 0 \to 0) + \frac{1}{3}\sigma(m = 1 \to 1). \tag{3.5}$$

In our applications, $\sigma(m = 0 \to 0)$ and $\sigma(m = 1 \to 1)$ are calculated separately and respectively in the subspaces with $m = 0$ and $m = 1$. For both calculations, the complex-rotated initial wavefunction is given by (3.1), where for the $m = 0 \to 0$ transitions we have

$$\Psi_i^\theta(u, v) = \mathrm{e}^{3\mathrm{i}\theta/2} R_{3p}\left(\frac{u+v}{2\lambda}\mathrm{e}^{\mathrm{i}\theta}\right)\sqrt{\frac{3}{2}}\frac{u-v}{u+v}, \tag{3.6}$$

for the $m = 1 \to 1$ transitions we have

$$\Psi_i^\theta(u, v) = -\mathrm{e}^{3\mathrm{i}\theta/2} R_{3p}\left(\frac{u+v}{2\lambda}\mathrm{e}^{\mathrm{i}\theta}\right)\frac{\sqrt{3uv}}{u+v} \tag{3.7}$$

and $R_{3p}(r)$ is the radial $3p$ state wavefunction of a sodium atom.

The results obtained by using following parameters: $\theta = 0.05$, $\lambda = 0.1$, $N_{\mathrm{DVR}} = 70 \times 70 = 4\,900$ and $N = 200\,000$ are shown at the bottom of Figure 2. They are in very good agreement with those of the R-matrix complex coordinate calculations of Seipp and Taylor [7], those of Harmin [22] obtained by the semiclassical approach and the experimental results of Luk *et al.* [21], shown in this order above our results in Figure 2.

Next, we again consider stepwise photoionization, but in an electric field of $F = 9.95$ kV/cm, where the first photon is right circularly polarized (σ^+) and takes the atom from the ground state to the pure $m = 1$ state of the $3p^2\mathrm{P}_{3/2}$ level. A second photon of σ^-, π or σ^+ polarization subsequently ionizes the atom above the (classical) ionization threshold located at $E \approx -611\ \mathrm{cm}^{-1}$. The dynamics in the final-state subspaces with $m = 0, 1, 2$ is relevant and the initial wavefunction is given by:

$$\Phi_i^\theta(u, v) = \frac{\mathrm{e}^{\mathrm{i}\theta}}{\sqrt{2}}\frac{\sqrt{uv}}{\lambda}\Psi_i^\theta(u, v) \tag{3.8}$$

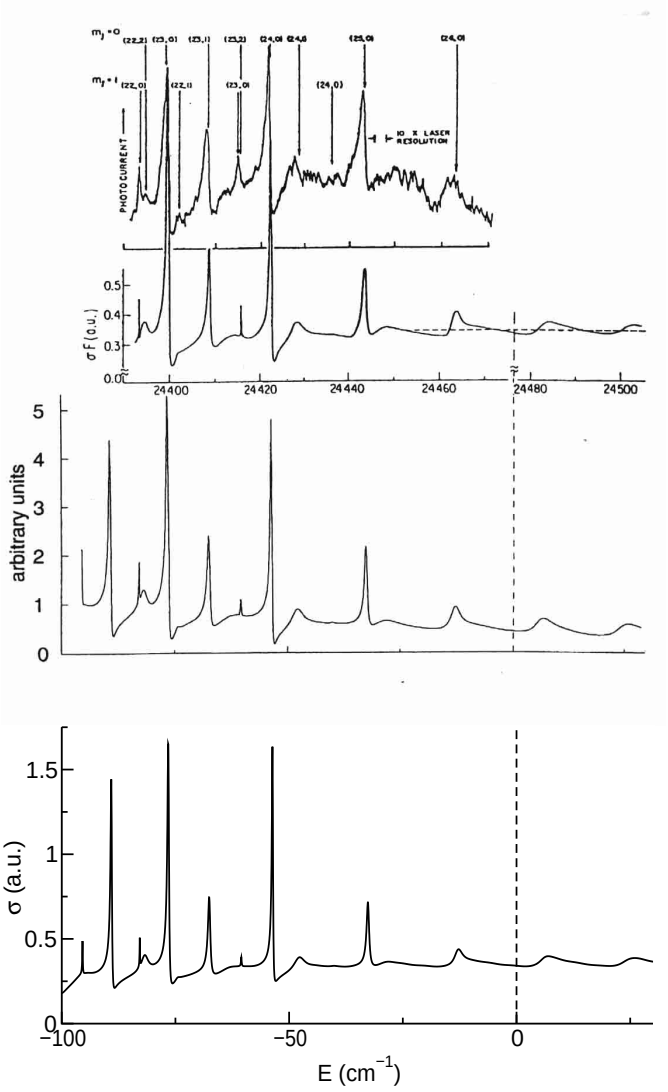

Fig. 2. $\pi\pi$-photoionization spectrum of Na from the ground state *via* $3p^2\mathrm{P}_{3/2}$ intermediate states in an electric field of $F = 3.59$ kV/cm. From the bottom to the top: present results, R-matrix complex coordinate calculations [7], semiclassical results [22] and experiment [21].

for $\sigma^\pm$ polarizations and by (3.1) for π polarization, with $\Psi_i^\theta(u, v)$ in all cases given by (3.7).

Our results, shown at the bottom of Figures 3, 4 and 5, have been obtained using the following typical set of parameters: $\theta = 0.05$, $\lambda = 0.1$, N_{DVR} from $70 \times 70 = 4\,900$ to $80 \times 80 = 6\,400$ and $N = 200\,000$. Since the $\sigma^+\sigma^+$ (Fig. 5) spectrum has very sharp peaks, in this case, we have again used the substitution $E \to E + \mathrm{i}\varepsilon$, with $\varepsilon = 0.04\ \mathrm{cm}^{-1}$. This value roughly corresponds to the width of 7.5×10^{-7} a.u. of the Gaussian used for the convolution of the results obtained by Seipp and Taylor [7]. As seen from Figures 3, 4 and 5 in all cases a satisfactory agreement is found with R-matrix complex coordinate calculations [7], semiclassical results [22] and experiment [23].

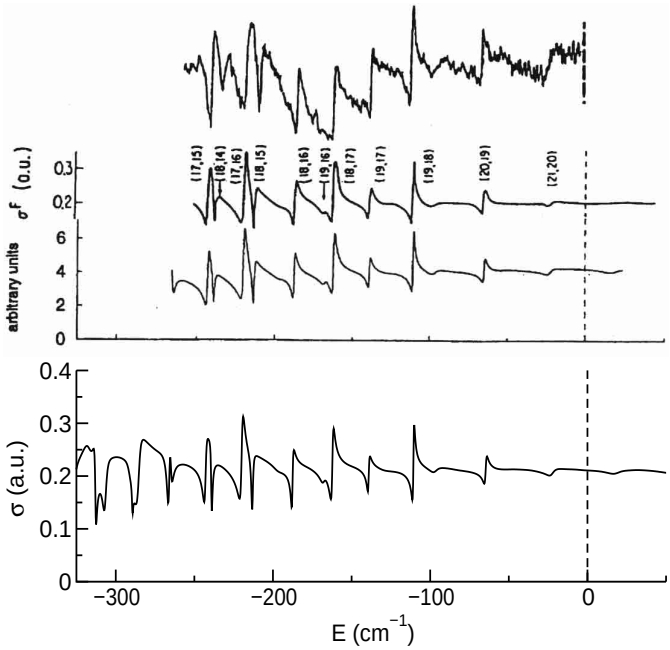

Fig. 3. $\sigma^+\sigma^-$-photoionization spectrum of Na from the ground state *via* a $3p^2\mathrm{P}_{3/2}$ intermediate state in an electric field of $F = 9.95$ kV/cm. From the bottom to the top: present results, R-matrix complex coordinate calculations [7], semiclassical results [22] and experiment [23].

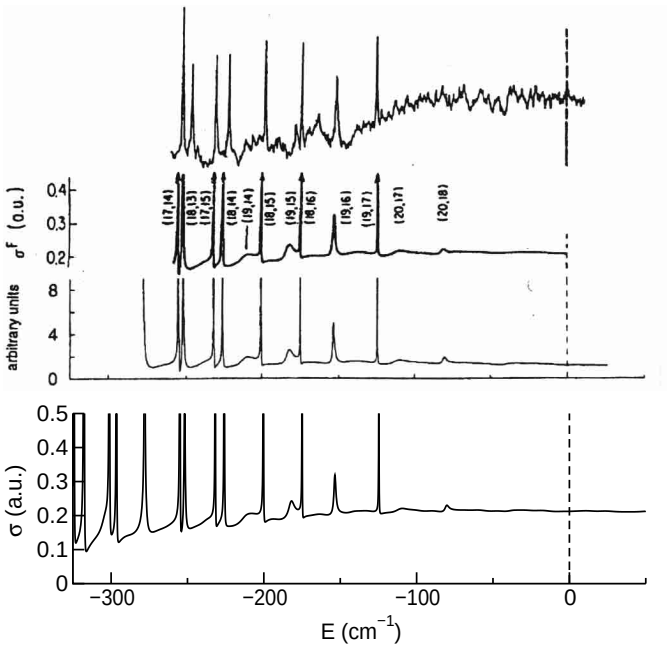

Fig. 4. Same as Figure 3 but for $\sigma^+\pi$ polarized photons.

3.3 Sodium atom in parallel electric and magnetic fields

We consider here the cases when the electric field strengths and photon polarizations are fixed to the values corresponding to those of Figures 2 and 3 and an additional parallel magnetic field is switched on.

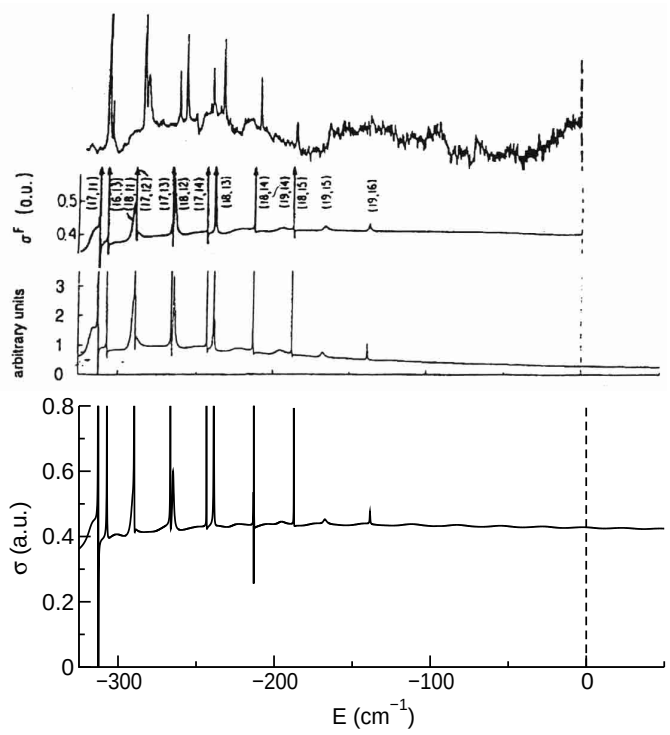

Fig. 5. Same as Figure 3 but for $\sigma^+\sigma^+$ polarized photons.

These kind of calculations have been previously performed by Seipp and Taylor using the complex-coordinate R-matrix method [7]. They have, however, neglected the paramagnetic interaction in the Hamiltonian (2.3) and in the case of the $\pi\pi$ transitions kept fixed contributions of the $m = 0 \to 0$ and $m = 1 \to 1$ transitions, like in relation (3.5). Under these assumptions, we have performed the same type of calculations for a series of increasing magnetic field strengths. The representative results for magnetic field strengths of $B = 5\times10^{-5}$ and $B = 2\times10^{-4}$ a.u. are shown in the middle of Figures 6 and 7, respectively. In order to obtain stable results with the increase of the magnetic-field strength, the number of DVR grid points is increased up to $N_{\mathrm{DVR}} = 140 \times 140 = 19\,600$ and the number of Lanczos iterations up to $N = 1\,000\,000$, with $\theta = 0.02$ and $\lambda = 0.07$. Spectra shown in the middle of Figures 6 and 7 are in fairly good agreement with the results of Seipp and Taylor [7] (top of the figures), although there are some differences in the peak intensities.

However, in a correct treatment, both, the paramagnetic term in Hamiltonian (2.3) used to describe final states and the influence of the magnetic field onto the intermediate state (that is a modification of relation (3.5)) have to be taken into account. The latter effect can be accounted for by applying a simple perturbation theory to the $3p^2$P-manifold of sodium-atom states in which the sum of the spin-orbit coupling and paramagnetic interaction is treated as perturbation. Then, assuming that the first laser is tuned to populate an intermediate state which is a linear combination of the $|m = 0, m_{\mathrm{s}} = 1/2\rangle$ and $|m = 1, m_{\mathrm{s}} = -1/2\rangle$ states, instead of the relation (3.5)

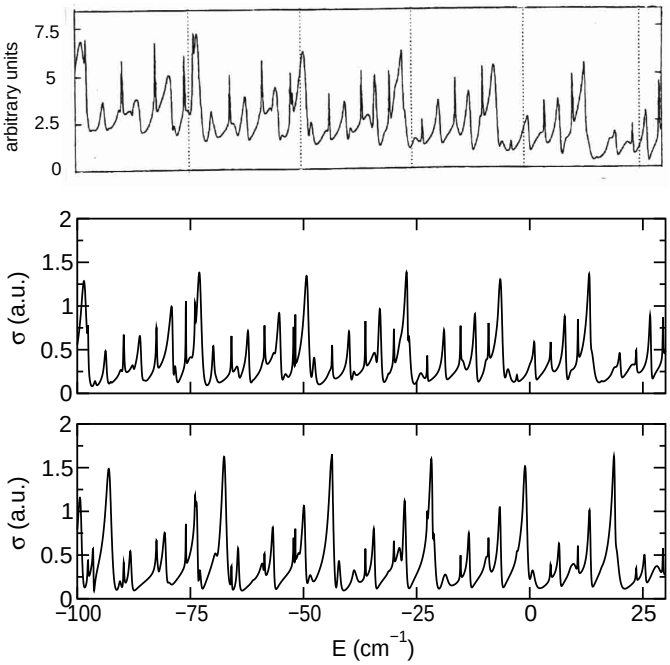

Fig. 6. $\pi\pi$-photoionization spectrum of Na from the ground state *via* a $3p^2$P intermediate state (which is a linear combination of $|m = 0, m_s = 1/2\rangle$ and $|m = 1, m_s = -1/2\rangle$ states) in an electric field of $F = 3.59$ kV/cm and parallel magnetic field of $B = 5 \times 10^{-5}$ a.u. At the bottom are our present results. In the middle and at the top are, respectively, our and the results of R-matrix complex scaling method [7], obtained by neglecting the perturbation of the intermediate state and the paramagnetic shift in the final states.

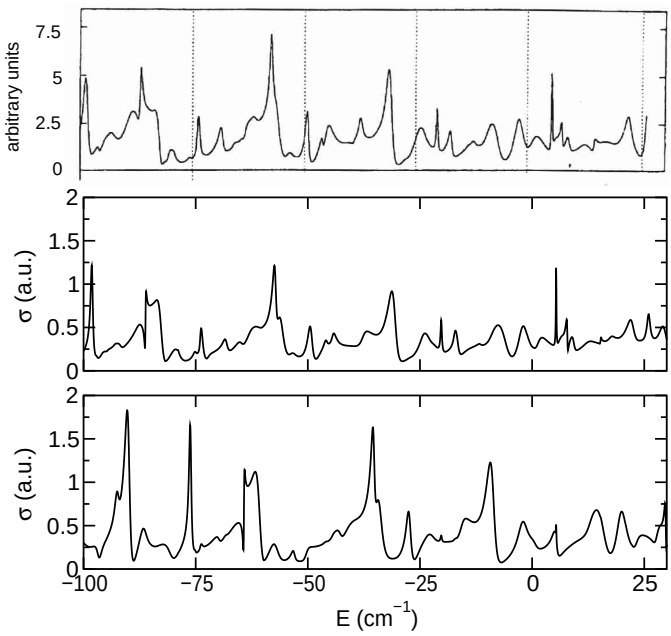

Fig. 7. Same as Figure 6, but for $B = 2 \times 10^{-4}$ a.u.

one finds for the photoionization cross-section:

$$\sigma = c_1(B)\sigma(m = 0, m_s = 1/2) + c_2(B)\sigma(m = 1, m_s = -1/2) \quad (3.9)$$

with

$$c_{1,2}(B) = \frac{1}{2}\left[1 \pm \frac{1+\beta}{[(1+\beta)^2+8]^{\frac{1}{2}}}\right] \quad (3.10)$$

where $\beta = B/A$ and $A = 11.33$ cm^{-1} [22] is the fine structure constant.

Using these relations, the calculated cross-sections are shown at the bottom of Figures 6 and 7. Comparing spectra in the middle and at the bottom of Figures 6 and 7, one can notice substantial differences. Reasons for this are that first, paramagnetic shifts in (2.3) are different for states with $(m = 0, m_s = 1/2)$ and $(m = 1, m_s = -1/2)$, and second, that coefficients $c_{1,2}(B)$ can differ substantially from their zero-magnetic-field limits $c_{1,2}(0) = 2/3, 1/3$.

In the case of the $\sigma^+\sigma^-$-spectra the intermediate state is characterized by $(m = 1, m_s = 1/2)$ and it is basically only necessary to properly account for the paramagnetic term in (2.3) corresponding to final states with $(m = 0, m_s = 1/2)$. Results of calculations, performed by using the same set of parameters as above, are shown in Figure 8 (the first and third spectra from the bottom). They compare well with the results of Seipp and Taylor [7] (the second and forth spectra from the bottom), when one takes into account that they have neglected an overall paramagnetic energy shift. Apart from this, just like in the case of the $\pi\pi$-spectra, some differences in peak intensities persist.

4 Concluding remarks

The method described in Section 2 can be successfully applied to the calculation of the total photoionization cross-sections of hydrogen and sodium atoms in electric and parallel electric and magnetic fields. The originality of our method is the combination of the DVR and the complex coordinate method. The use of DVR has numerous advantages. The potential energy matrix is diagonal and can be trivially obtained. Core potential of a non-hydrogenic atom can be easily introduced. For multidimensional problems, the kinetic energy matrix is sparse, so that efficient matrix-vector multiplication codes can be developed. They are prerequisites for an overall efficient iterative procedure.

When compared with the existing methods of computation, our method is characterized with minimal memory requirements – just a few vectors of dimension N_{DVR}. This is a direct consequence of the above listed properties of a DVR.

However, as we have found out in our calculations, the number N of Lanczos iterations (*i.e.* CPU time) necessary for the convergence increases significantly with N_{DVR} – the DVR basis size. Thus, to obtain spectra in Figure 1 ($N_{\mathrm{DVR}} = 4\,900$, $N = 200\,000$) we needed 12 minutes of CPU time on an IBM RS6000/Power3 workstation, while to obtain those in Figure 7 corresponding to the strongest

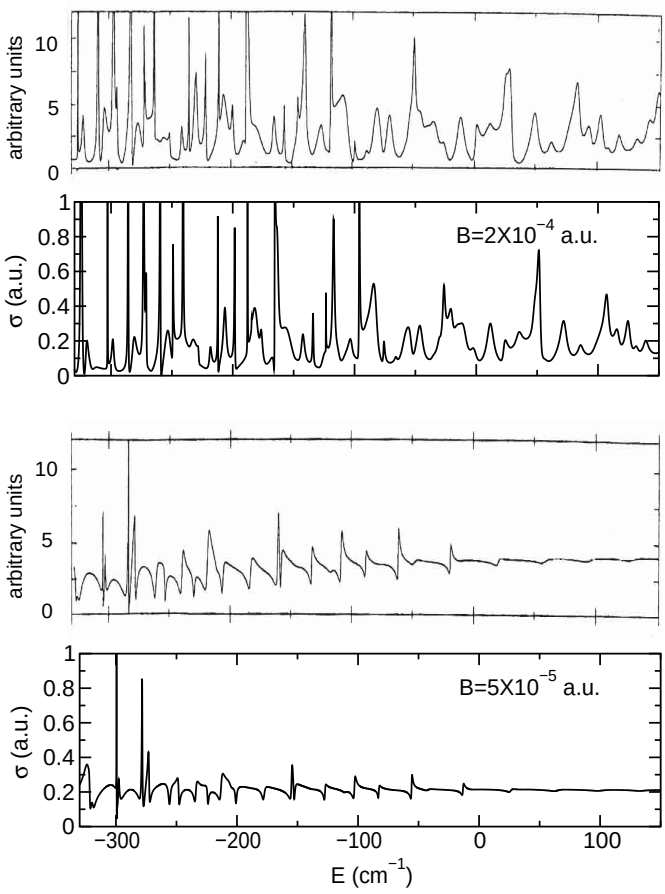

Fig. 8. $\sigma^+\sigma^-$-photoionization spectrum of Na from the ground state *via* a $3p^2$P intermediate state (characterized by $m = 1$, $m_s = 1/2$) in an electric field of $F = 9.95$ kV/cm and parallel magnetic fields of $B = 5 \times 10^{-5}$ to $B = 2 \times 10^{-4}$ a.u. Present results are given as the first and third spectra from the bottom, whereas the results of R-matrix complex scaling method [7] are given as the second and the forth.

magnetic field ($N_{\mathrm{DVR}} = 19\,600$, $N = 1\,000\,000$) we needed 24 hours of CPU time. Apparently, with the increase of magnetic field strength, the density of (overlapping) resonances increases and to correctly represent them, we need a larger DVR basis. Larger basis generates larger spectral range of the Hamiltonian matrix and just like in other iterative procedures (see for example Ref. [16]) the number of necessary iterations is directly proportional to the product of the spectral range and the density of states.

References

1. W.P. Reinhardt, Ann. Rev. Phys. Chem. **33**, 223 (1982).
2. T.N. Rescigno, V. McKoy, Phys. Rev. A **12**, 522 (1975).
3. G. Alvarez, R.J. Damburg, H.J. Silverstone, Phys. Rev. A **44**, 3060 (1991).
4. D. Delande, A. Bommier, J.C. Gay, Phys. Rev. Lett. **66**, 141 (1991).
5. J. Main, G. Wunner, J. Phys. B **27**, 2835 (1994).
6. M.H. Halley, D. Delande, K.T. Taylor, J. Phys. B **26**, 1775 (1993).
7. I. Seipp, K.T. Taylor, J. Phys. B **27**, 2785 (1994).
8. G. Moro, J.H. Freed, J. Chem. Phys. **74**, 3757 (1981).
9. C. Lanczos, J. Res. Natl. Bur. Std. **45**, 255 (1950).
10. R. Haydock, Solid State Phys. **35**, 216 (1980).
11. H.O. Karlsson, O. Goscinski, J. Phys. B **27**, 1061 (1994).
12. H.O. Karlsson, O. Goscinski, Phys. Rev. A **51**, 1154 (1995).
13. J.C. Light, I.P. Hamilton, J.V. Lill, J. Chem. Phys. **82**, 1400 (1985).
14. D. Baye, P.H. Heenen, J. Phys. A **19**, 2041 (1986).
15. H. Suno, L. Andric, T.P. Grozdanov, R. McCarroll, Phys. Lett. A **265**, 377 (2000).
16. T.P. Grozdanov, L. Andric, C. Manescu, R. McCarroll, Phys. Rev. A **56**, 1865 (1997).
17. H. Suno, L. Andric, T.P. Grozdanov, R. McCarroll, Phys. Rev. A **59**, 524 (1999).
18. W.H. Press, B.P. Flannery, S.A. Teukolsky, W.T. Vetterling, *Numerical Recipes* (Cambridge University Press, Cambridge, 1986).
19. M. Klapisch, Thèse de Doctorat, Université Paris-Orsay, 1969.
20. H. Rottke, K.H. Welge, Phys. Rev. A **33**, 301 (1986).
21. T.S. Luk, L. DiMauro, T. Bergeman, H. Metcaf, Phys. Rev. Lett. **47**, 83 (1981).
22. D.A. Harmin, Phys. Rev. A **26**, 2656 (1982).
23. S. Feneuille, S. Liberman, E. Luc-Koenig, J. Pinard, A. Taleb, Phys. Rev. A **25**, 2853 (1982).